Vibrational levels of the transition state and rate of dissociation of triplet acetaldehyde

Gen-Hou Leu, Cheng-Liang Huang, Shih-Huang Lee, Yu-Chang Lee, and I-Chia Chen[a)]
Department of Chemistry, National Tsing Hua University, Hsinchu, Taiwan 300, Republic of China

(Received 29 June 1998; accepted 28 August 1998)

Fluorescence decay of the S_1 state of d_4-acetaldehyde is measured. Below the dissociation threshold for formation of fragments of formyl and methyl radicals, single exponential decays of fluorescence are observed. Biexponential decay is observed when the excitation energies are near and above the dissociation threshold. Hence, in this region the mechanism for intramolecular relaxation of energy reaches the ''intermediate case.'' Strong coupling between S_1 and T_1 states or reversible reaction for $S_1 \leftrightarrow T_1$ results in this biexponential behavior in the fluorescence decay of S_1. Rates of appearance of DCO from dissociation of acetaldehyde are measured. The stepwise increases in plots of both rate of appearance of formyl radicals and rate of decay of excited acetaldehyde versus excitation energy for both isotopic variants of acetaldehyde are observed. According to fits to Rice–Ramsperger–Kassel–Marcus (RRKM) theory, these sharp increases correspond to vibrational levels of transition state in the triplet surface. Frequencies of torsional and C–C–O bending modes are determined to be (73 ± 10) and (200 ± 10) cm^{-1} for the transition state of CD_3CDO and the torsional frequency (80 ± 10) cm^{-1} for CH_3CHO. That these fitted frequencies are less than values calculated with methods B3LYP and MP2 indicates a looser transition state than calculated for dissociation. From these fits the dissociation threshold for formation of radical fragments is determined to be 31 845 for CD_3CDO and 31 650 cm^{-1} for CH_3CHO. © *1998 American Institute of Physics.* [S0021-9606(98)02545-8]

I. INTRODUCTION

The photochemistry and photophysics of acetaldehyde have been studied extensively. A molecule of this moderate size serves as a convenient link to understand detailed dynamics from small molecules to large carbonyl compounds. We investigate the mechanism of photodissociation and relaxation of acetaldehyde in the ultraviolet (UV) region. In this range acetaldehyde is excited to a state S_1 through an $n-\pi^*$ transition. Previous work[1,2] showed that at low vibrational energy of the S_1 state, the main mechanism of decay involves internal conversion to highly vibrationally excited states of S_0. From the results of quantum-beat experiments,[3,4] interaction of S_1 and T_1 states is observed when some T_1 states have energies near those of a S_1 state. The T_1 state correlates with formation of radical products $HCO+CH_3$ with a small exit energy barrier, according to results of both experimental[4–8] and theoretical studies.[9] This radical channel was proven to be the major process for dissociation of acetaldehyde after photolysis in the UV region.[10,11] Above the dissociation threshold, the process of intersystem crossing to T_1 becomes a major energy dissipating process for excited acetaldehyde. A schematic diagram of low-lying electronic states of acetaldehyde appears in Fig. 1.

Relaxation of the S_1 state of acetaldehyde can be detected by monitoring the rate of fluorescence decay. Biexponential decay is observed in an energy range near the dissociation threshold for formation of radical products.[4,12] This behavior of an ''intermediate case'' for intramolecular energy relaxation is caused by coupling of the triplet state to some dissociating channel so that the lifetime of these triplet states is decreased and the density of states is increased. The number of molecular eigenstates within the laser resolution

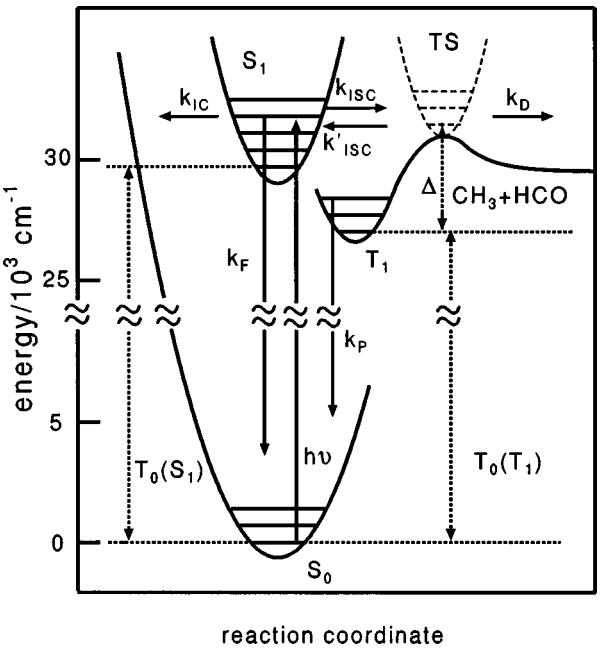

FIG. 1. Schematic diagram of potential energy surfaces of low-lying electronic states of acetaldehyde and their correlations with products.

a)Author to whom all correspondence should be addressed; electronic mail: icchen@chem.nthu.edu.tw; fax number: 886-3-5721614.

increases; the resulting decay of several eigenstates can be fitted by a biexponential function. Measurement of relaxation rates of the S_1 state of both h_4- and d_4-acetaldehyde is important in investigating the isotopic effects in crossing rates between the S_1 and T_1 states and their correlation with dissociation channels.

Formyl radicals as products are sensitively detected by laser-induced fluorescence (LIF) on the transition $\tilde{B}\ ^2A' - \tilde{X}\ ^2A'$ to indicate the relative yield of this fragment as a function of vibrational energy in the S_1 state and the appearance rate of fragmentation.[13–18] The Rice–Ramsperger–Kassel–Marcus (RRKM) theory successfully describes the rates of dissociation of triplet ketene,[19,20] NO_2,[21] etc. In this theory one assumes that vibrational energy flows freely among various degrees of freedom at a rate much greater than the reaction rate. The microcanonical ensemble version of transition state theory for the rate of unimolecular reaction shows that the dissociation rate coefficient is $k = W/h\rho$, in which W is a sum over transition states, h is Planck's constant, and ρ is the density of dissociating states.[22] Near the dissociation threshold, according to this theory, the dissociation rate is expected to increase sharply. Some stepwise increases correspond to vibrational levels orthogonal to the reaction coordinate in transition states.[19–21,23] The structures of transition states were studied using various techniques.[24–26] This is important for the understanding of reaction dynamics and to test the theory of unimolecular dissociation.

In the present work the rate of dissociation of deuterated acetaldehyde is measured by detecting the fragment DCO and decay rate of the S_1 state. Comparison with results from RRKM theory is made to resolve vibrational levels of the transition state along the triplet channel.

II. EXPERIMENT

Acetaldehyde (Aldrich, 99.5%) was purified by vacuum distillation and Ar was added to make a 15% mixture (CH_3CHO/Ar). Deuterated acetaldehyde (Aldrich, 99%) was used directly without purification and a 10% mixture in argon (CD_3CDO/Ar) was made. These mixtures were expanded through a pulsed nozzle (General Valve, diameter 0.8 mm) operating at a repetition rate 10 Hz with a stagnation pressure ~1000 Torr to form the supersonic jet. Argon was used as a buffer gas to decrease the velocity of the molecular jet so as to enable detection of the entire decay of fluorescence and to obtain long rise curves for measurement of the appearance of formyl radicals.

A. Fluorescence decay of acetaldehyde

A dye laser (Continuum ND60, dual gratings, DCM and DCM special dyes) pumped by a Nd:YAG laser (Continuum NY81C) serve to excite acetaldehyde to the S_1 state. The wavelength range of the laser after the doubling crystal is 310–336 nm, with resolution $\Delta\omega \approx 0.10\ cm^{-1}$, pulse energy 4–6 mJ/pulse, and temporal pulse width 7 ns. About 2 cm downstream from the orifice of the pulsed valve, the laser pulses interacted with the molecular jet to excite acetaldehyde. In the region of interaction, the laser pulses were polarized vertically and the beam diameter was ~6 mm.

The absolute wavelength of laser pulses was calibrated with I_2 transitions. Cut-off filters (Schott 335, 345, and 360) attenuated the scattered light. Traces of fluorescence decay were recorded with fixed laser wavelength. A lens (f/1, diameter 2″) in combination with a second lens to focus the emission onto a viewing window (diameter 3 cm) further decreased scattered light. The signal without dispersion was detected with a photomultiplier (EMI 9828QB) having a response time 2 ns and a cathode of active diameter 2″. A digital oscilloscope (8-bit, LeCroy 9450) was used to obtain the emission traces at a sampling rate 400 MHz and resolution 2.5 ns. About 1000 laser shots were averaged for each trace. The scattered light was diminished with baffles on two side arms of the reaction chamber and with optical filters. Background noise was tested using only argon in the molecular jet to measure Rayleigh scattering from interaction with the laser pulses;[27] negligible contribution to the signal resulted from this process. Decay traces up to 10 μs were acquired. Under these experimental conditions, the proportion of excited molecules leaving the detection zone within 10 μs is negligible.

B. Detection of formyl radical

A second dye laser (Lambda Physik LPD-3002) pumped with a Nd:YAG (Continuum NY82) generated pulses 10–15 mJ near wavelength 516 nm (dye coumarin 500). The frequency was doubled in a BBO crystal to give a UV beam with energy 1–2 mJ/pulse at resolution ~0.2 cm^{-1} to excite HCO or DCO to the $\tilde{B}\ ^2A'$ state. The photolysis and probe laser pulses overlapped spatially in the interaction region to enable detection of the nascent fragment HCO or DCO from acetaldehyde after photolysis; in this region, the area of the probe beam was 8 mm^2. The photolysis and horizontally polarized probe laser pulses were counterpropagating and orthogonal to the molecular jet. Total fluorescence of formyl radicals was detected with a different photomultiplier (EMI 9658R) mounted at right angles to the jet and both laser beams. A fast preamplifier amplified the signal ten times. Because HCO or DCO emits at a wavelength smaller than that of the photolysis pulse, the wavelength range for detection was made small so as to minimize the scattered light and emission from excited acetaldehyde. For this purpose a cut-off filter (Schott, WG 335) and an interference filter [CVI (334 ± 10) nm) were used.

The rise curves of fragment HCO or DCO were recorded on fixing the wavelength of the probe beam to one of HCO or DCO transitions and varying the delay between the two laser pulses. The integrating gate in the boxcar was set to cover the full scanning range. In this way the flat background noise includes emission from excited acetaldehyde produced from photolysis pulses. Each recorded curve was summed over six scans in total from both directions; for each scan about 20 laser shots were averaged for each data point. With delays greater than 2 μs, products began to move beyond the region of detection of the probe laser pulses; the fluorescence intensity of HCO/DCO consequently decreased.

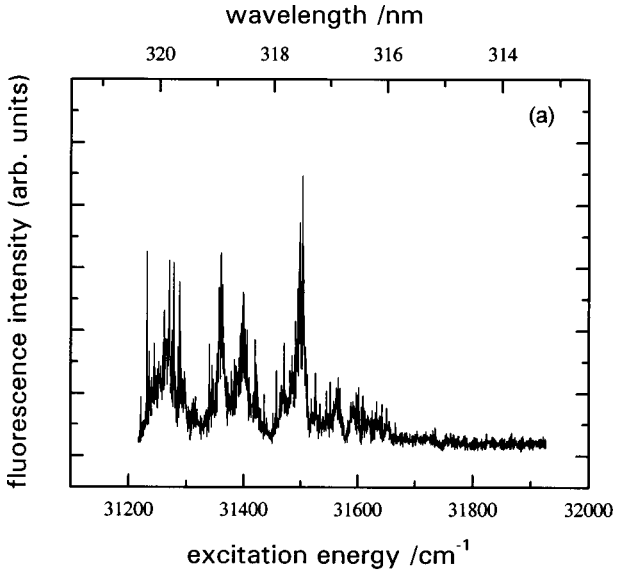

FIG. 2. (a) Flourescence excitation spectrum of CH_3CHO S_1-S_0 transition in the wavelength range 313–321 nm, and (b) PHOFEX spectrum for CH_3CHO monitoring the flourescence yield and fixing the probe beam at transition ${}^{Q}R_0(10)$ of HCO.

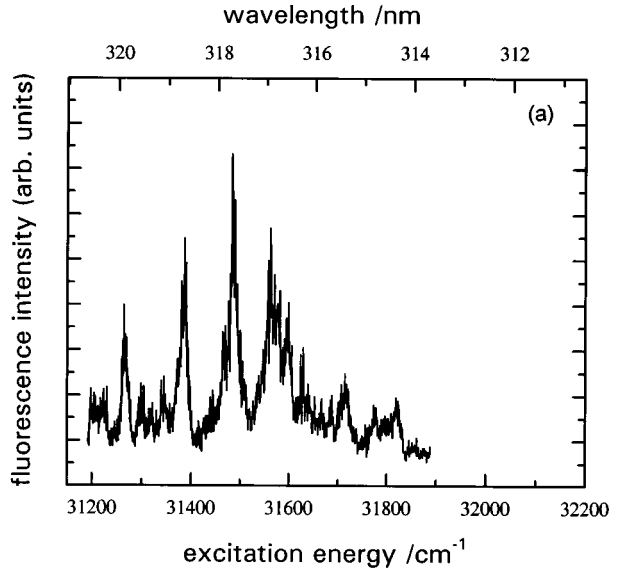

FIG. 3. (a) Flourescence excitation spectrum of CD_3CDO S_1-S_0 transition in the wavelength range 313–321 nm, and (b) PHOFEX spectrum of CD_3CDO monitoring the fluorescence yield of DCO. The probe beam is fixed at transition ${}^{Q}R_1(4)+(5)$ of DCO, shown in Fig. 4.

III. RESULTS

A. Spectra of S_1-S_0 transition of acetaldehyde

The fluorescence excitation spectrum of CH_3CHO near the dissociation threshold, shown in Fig. 2(a), was recorded in the wavelength range 313–321 nm on scanning the excitation laser. Spectra of CH_3CHO and CD_3CDO at low energy near the zero point of $\tilde{A}\ {}^1A''(S_1)$ are studied in detail.[28–35] However, because there are small barriers to inversion of acetyl hydrogen and to torsional motion of methyl moiety, and because there is interaction between these two vibrational motions and also with rotation of the molecule, definite spectral assignments are not attainable for highly vibrationally excited states of S_1. Weak fluorescence observed below wavelength 317 nm for CH_3CHO confirms the predissociation character of the S_1 state. A photofragment excitation (PHOFEX) spectrum of CH_3CHO displayed in Fig. 2(b) was obtained on monitoring the yield of total fluorescence of HCO with the probe laser fixed on the transition ${}^{Q}R_0(10)\tilde{B}\ {}^2A'-\tilde{X}\ {}^2A'$ of HCO. This spectrum is essentially equivalent to the absorption spectrum if the dissociation yield is uniform throughout the detected wavelength region. Hence these two spectra shown in Figs. 2(a) and 2(b) have similar structure except that at wavelengths less than 317 nm the fluorescence yield of CH_3CHO decreases; this position corresponds to the threshold for formation of $HCO+CH_3$ as reported previously.[4,36,37] In both spectra the intensity was not normalized to power fluctuations of laser beams.

Fluorescence excitation and PHOFEX spectra of CD_3CDO are shown in Figs. 3(a) and 3(b), respectively. The latter spectrum was acquired on monitoring DCO at a transition indicated with an arrow shown in Fig. 4. Rotational

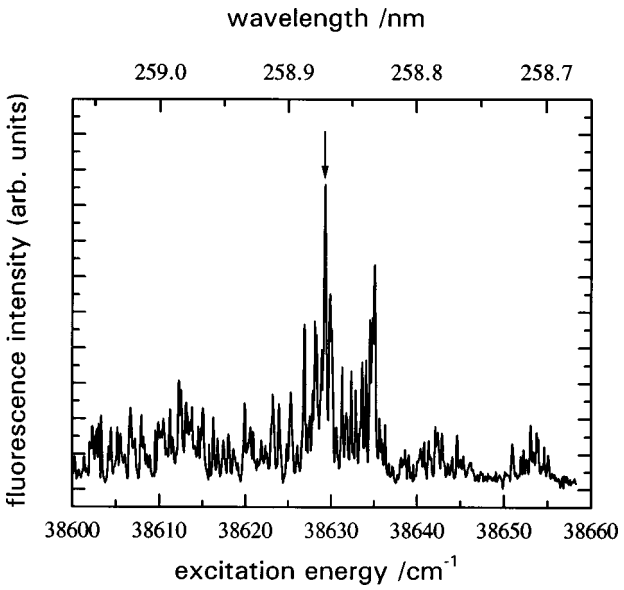

FIG. 4. Laser-induced fluorescence excitation spectrum of band $\tilde{B}\ ^2A' - \tilde{X}\ ^2A'\ 0_0^0$ of DCO. DCO was produced from CD_3CDO after photolysis at wavelength 310.7 nm. The arrow indicates the position of the probe beam to acquire the rise curves of DCO and PHOFEX spectrum of CD_3CDO.

structure of transition $\tilde{B}\ ^2A' - \tilde{X}\ ^2A'$ of DCO similar to that of HCO was observed. The analyses of rotational states are reported in the literature.[38] At energies above the dissociation threshold for production of radicals, PHOFEX spectra of both isotopic variants of acetaldehyde display partially resolved rotational structure in the $S_1 - S_0$ transition.

B. Fluorescence decay of acetaldehyde

Some experimental data on CH_3CHO from previous work[4,35] are displayed in Figs. 6 and 8(a) to compare with results from the isotopic variant CD_3CDO. At a vibrational energy near the zero point of the S_1 state, the fluorescence decay was measured on fixing the laser wavelength at a rovibronic transition. Most curves display single exponential behavior except that some curves display oscillation due to interaction with T_1 states. The decay time coefficient of CD_3CDO was measured to be 3–3.6 μs less than that of the S_1 state of CH_3CHO with similar vibrational energy. The reason is that Franck–Condon factors for overlap of S_1 and S_0 states are less favorable for the deuterated species. A shorter decay about 1.5–2 μs for CD_3CDO was reported by Noble and Lee,[39] probably due to loss of excited molecules from the detecting zone.

In the wavelength range 312–320 nm, in which the spectrum is congested, the decays of CD_3CDO were taken at an interval of 0.05 nm, despite partially resolved rotational structure. These decay curves exhibit biexponential behavior. At wavelengths less than 316.4 nm, a third component with a time constant ~3 μs appears. Figure 5 shows some experimental curves of fluorescence decay of CD_3CDO. An energy of the excitation laser decreased to less than 1 mJ/pulse was used to test for a possible contribution to the rapid component from Rayleigh scattering.[27] The variation of relative

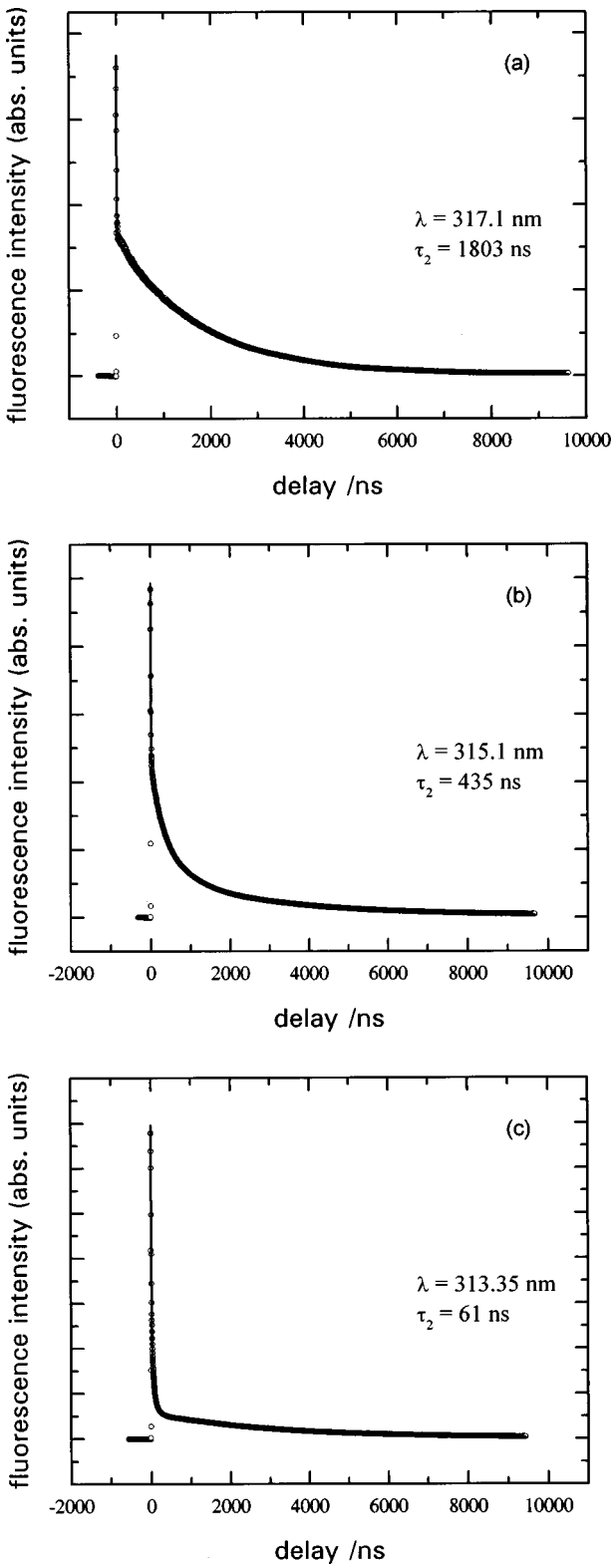

FIG. 5. Fluorescence decays of CD_3CDO at excitation wavelength λ (a) 317.1, (b) 315.1, and (c) 313.35 nm and the fitted exponential curves with time coefficient (a) 8 and 1803 ns (b) 7 ns, 435 ns, and 3.31 μs, and (c) 8 ns, 61 ns, and 3.44 μs. The second time coefficient τ_2 is shown in the plots.

amplitude from using less laser power for the fast and slow components of decay curves is small and less than experimental uncertainty. Because of spectral congestion and because a relatively warm jet was used, more transitions were-

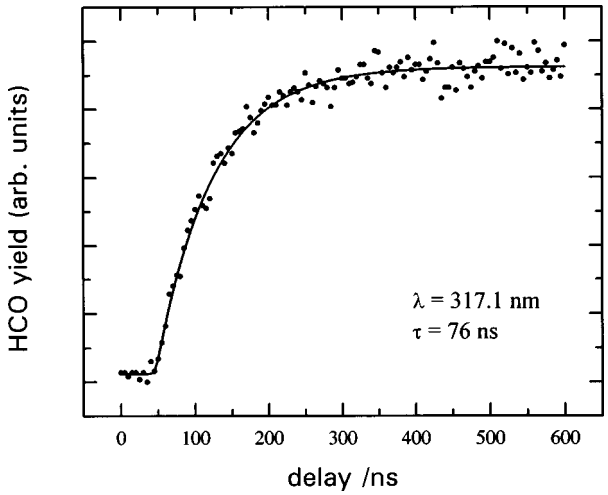

FIG. 6. Measured rise curve of HCO LIF intensity after photolysis of CH_3CHO as a function of delay between photolysis and probe laser pulses. The zero of abscissa is set arbitrarily and is not equal to zero delay between pulses. The photolysis wavelength is 317.10 nm, the monitored transition is $^QR_0(10)$, and the fitted time coefficient of rise is 76 ns.

accessible; contribution from Rayleigh scattering was insignificant compared to the intense signal observed in this work.

C. Rate of appearance of formyl radicals

The transition $^QR_0(10)$ was used to monitor the yield of HCO formed as a function of delay between photolysis and probe laser pulses in the wavelength range 312–319 nm for photolysis.[4] Figure 6 presents an experimental rise curve of fluorescence of HCO from acetaldehyde after photolysis; the photolysis wavelength is 317.1 nm and the fitted time coefficient to a single exponential rise function is 76 ns. No variation of this coefficient was discerned on monitoring the transition $^QR_0(10)$ and the head of the branch $^QR_0$. Rise curves of fluorescence intensity of HCO show a single exponential characteristic; the rate of appearance increases with decreasing wavelength of excitation. The yield of DCO as a function of decay time was measured on monitoring the transitions of DCO at $^QR_1(4)+(5)$; those rise curves appear in Fig. 7. All curves measured within 2-μs range have single exponential behavior. The rates of appearance of HCO and DCO plotted as a function of photolysis wavelength are displayed in Figs. 8(a)[4] and 8(b), respectively. Both plots have a sharp increase near 316 and 314 nm for HCO and DCO appearance, respectively, and stepwise structures with sharp increases greater than experimental uncertainties.

IV. ANALYSIS AND DISCUSSION

A. Fits of decay curves to exponential functions

Previous work[4] showed that under similar experimental conditions, near and above the dissociation region, most curves for decay of CH_3CHO fluorescence display biexponential behavior. For CD_3CDO near the dissociation threshold, the decay curves display biexponential behavior. All the measured decay curves were fitted to exponential functions. Deconvolution of the laser pulse width was performed for curves with rapid decay. At excitation wavelengths less than

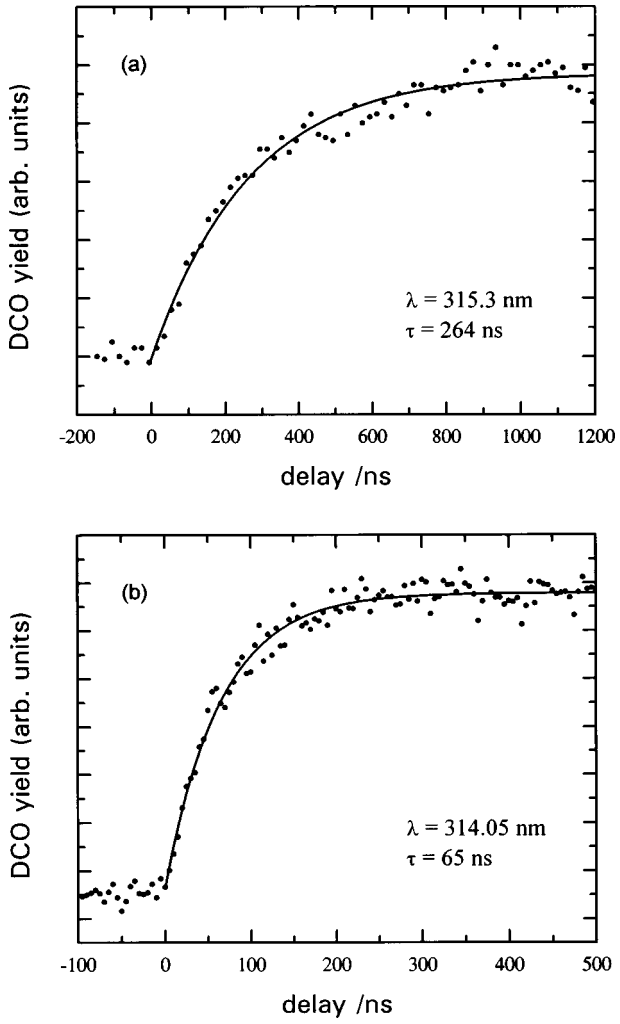

FIG. 7. Measured rise curves of DCO LIF intensity after photolysis of CD_3CDO at wavelength (a) 315.30 and (b) 314.05 nm as a function of delay between photolysis and probe laser pulses. The fitted curves are single exponential functions.

316.4 nm, the measured decay curves can not be fitted with biexponential functions. A third component appears with a relatively small amplitude. In this case a triexponential function was used to fit the experimental curves. This function is defined to be

$$I(t)=A_1e^{-k_1t}+A_2e^{-k_2t}+A_3e^{-k_3t}, \tag{1}$$

in which A_1, A_2, and A_3 represent the amplitudes and k_1, k_2, and k_3 represent the rate coefficients for fast, intermediate, and slow components, respectively. For a biexponential decay, only the first two terms were included. For all measured curves, the fitted rate coefficients k_1 for the fast components vary in the range $1.5-1\times10^8$ s^{-1} in the wavelength range 317–312 nm. k_1 shows no dependence on vibrational energy for S_1.

For those curves displaying triexponential decay, the fitted time coefficients for the slow components $1/k_3$ are ~3 μs and remain constant through the wavelength range of detection. The lifetime of the slow component is similar to the lifetimes of states near the zero point of S_1. A similar phenomenon was observed for CH_3CHO for which a slow component appears at short excitation wavelengths.[4] Ohta *et al.*[40]

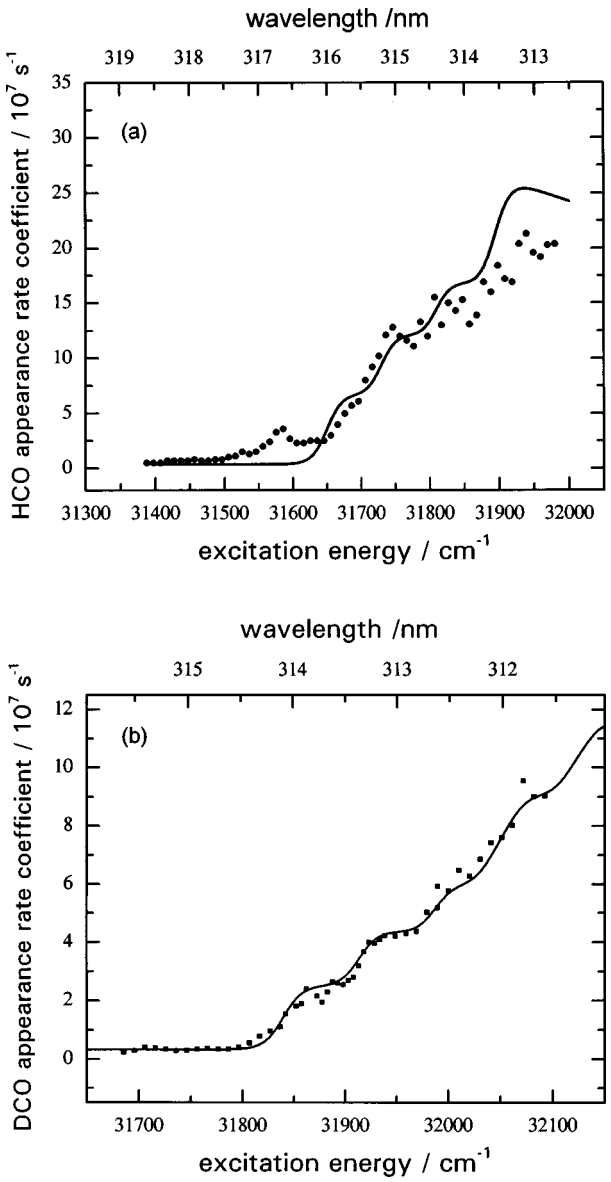

FIG. 8. Rate coefficients of appearance of (a) HCO and (b) DCO from acetaldehyde versus excitation energy and the RRKM fit in solid line. These fits assume an imaginary frequency $60i$ cm^{-1} for the transition state of both isotopic variants.

observed analogous slow component for CD_3CDO and proposed a formation of complexes during expansion of the jet. The fitted amplitudes for varied excitation wavelengths, shown in Fig. 9, show that the amplitude A_3 seems not to depend on excitation wavelength. However, there is a linear correlation of amplitude A_1 and A_2 to the PHOFEX spectral intensity; the A_1 and A_2 values increase when absorption of acetaldehyde increases. Figure 10 shows the ratio A_1/A_2 as a function of excitation energy indicating that the preexponential factor A_2 decreases abruptly near 313.5 nm.

Increasing the distance between the interaction region of excitation pulses with the molecular jet to the outlet of a pulsed nozzle is expected to cool the molecules further and to decrease the rate of collision; less excited acetaldehyde is thereby expected to relax to lower levels of S_1 states via collision. However, the amplitude of the slow component

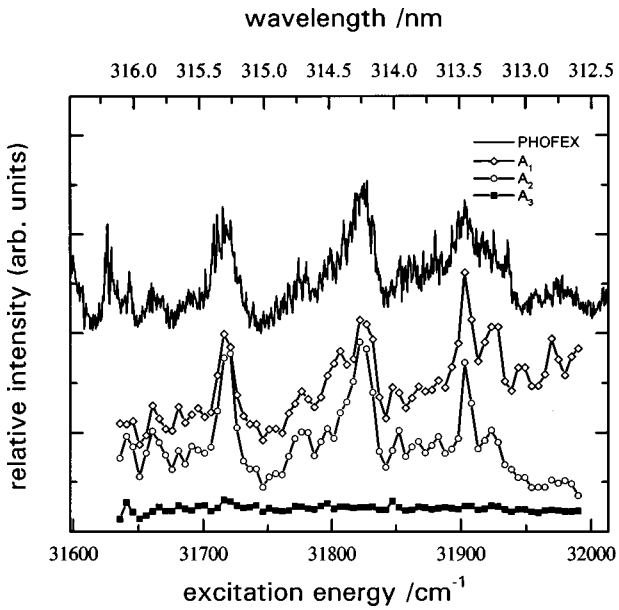

FIG. 9. Relative amplitudes A_1, A_2, and A_3 obtained from fitting the decay curve of CD_3CDO fluorescence versus excitation energy and comparison with PHOFEX spectrum.

does not decrease on further cooling the molecular jet. For emission from acetaldehyde in a gas cell under low pressure, the slow component disappeared. Complex formation in a supersonic jet is generally observed when argon is used as a carrier gas. Most likely complexes were formed during expansion of the beam and were excited with the laser, then underwent dissociation to form product acetaldehyde in an excited S_1 state with small vibrational energy. In this way the observation of a slow decay with a rate coefficient similar to that of S_1 acetaldehyde can be explained.

The fitted second rate coefficient k_2 versus excitation energy is displayed in Figs. 11 and 12. It increases abruptly at a wavelength ~316 for CH_3CHO and ~314 nm for CD_3CDO. In addition, stepwise increases in a rate coefficient

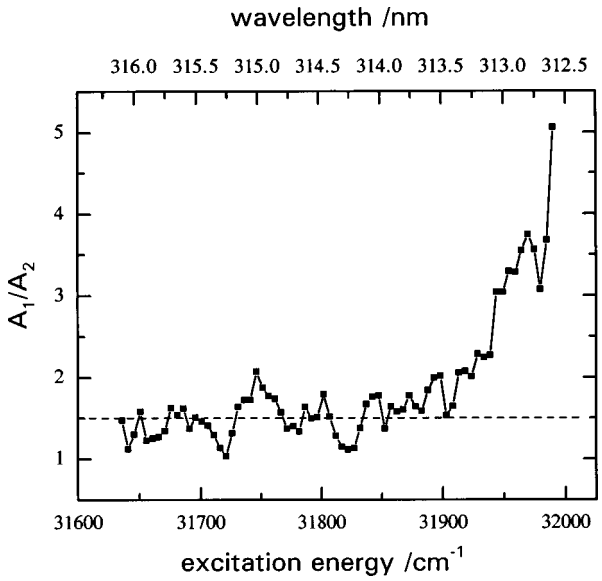

FIG. 10. Plot of ratio A_1/A_2 versus excitation energy.

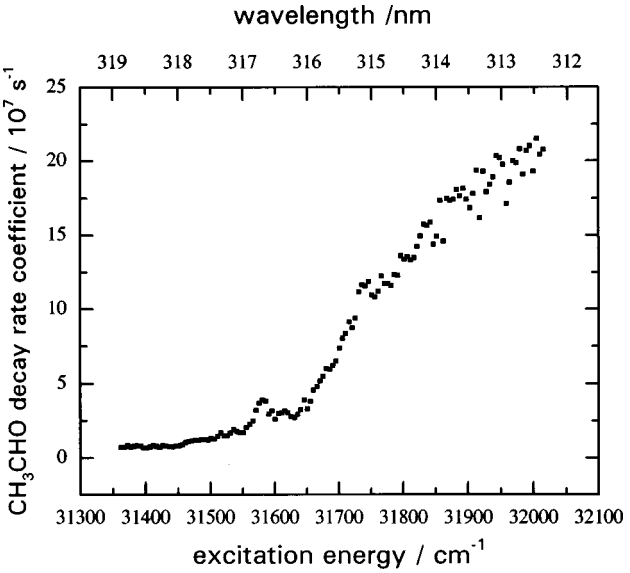

FIG. 11. Plot of fitted rate coefficient for the slow component in the emission decay of CH_3CHO versus excitation wavelength.

consistent with steps in the rate of appearance of formyl radical are observed. These sharp steps correspond to no major vibronic bands in PHOFEX spectra. At wavelengths less than ~314 nm, k_2 is less than the rate of appearance of DCO at the same excitation wavelength. In the case of CH_3CHO, the decay rate coefficient k_2 of the slow component approximately equals the rate coefficient for the appearance of HCO, from comparison of Figs. 11 and 8(a).

B. Dynamics of excited acetaldehyde

Results of experiments show that both isotopic variants of acetaldehyde display biexponential decay in their fluorescence intensity at high vibrational energy in S_1. This phenomenon is explained as an ''intermediate case'' for intramolecular relaxation of energy. According to a theory derived by Kommandeur and co-workers[41–43] and by Lahmani *et al.*,[44,45] the fast rate corresponds to dephasing of the bright state, S_1, and the slow process is the decay of molecular eigenstates formed from mixing S_1 and T_1 states. According to a chemical–kinetic model, this biexponential behavior is due to a reversible process between S_1 and T_1 states; the fast component is related to intersystem crossing for S_1 to T_1 and the slow one is from $T_1 \rightarrow S_1$. The ratio of amplitudes of these biexponential terms A_1/A_2 approximately equals the number of coupling states N. From previous work[3,4] the coupling states are T_1 states. Figure 9 shows a plot of the ratio A_1/A_2 vs excitation energy. At a small excitation energy, the ratio is slightly greater than unity, indicating that on average about 1–2 T_1 states are coupled to the excited S_1 state. A sudden increase of the ratio observed near wavelength ~313.5 nm indicates an increase of coupling states N or depleting of the T_1 population. Hence this position indicates where the T_1 state starts to interact with a dissociation continuum.

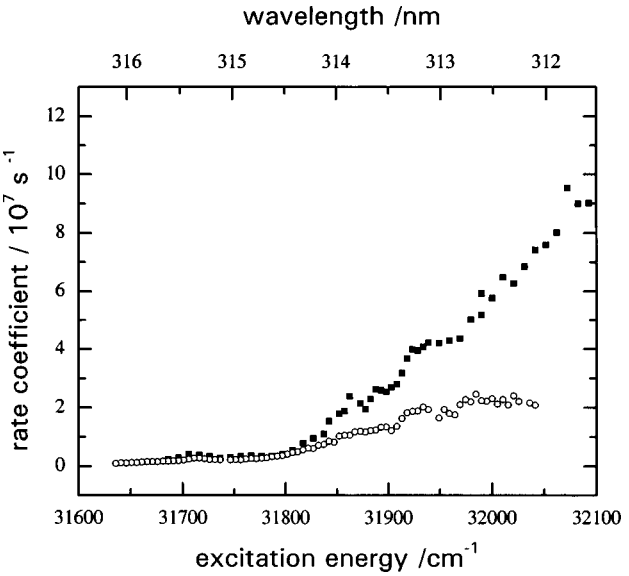

FIG. 12. Fitted rate coefficient k_2 of the slow component in the emission decay of CD_3CDO versus excitation wavelength shown in (■) and rate coefficient for the appearance of DCO from acetaldehyde after photolysis plotted as a function of photolysis wavelength (○).

From the results of Kommandeur and co-workers,[41–43] at the limit of strong coupling, the rate coefficient k_1 is explained as reflecting the dephasing rate of S_1. According to the experimental data, this dephasing rate of CD_3CDO is about twice as great as that for CH_3CHO, which is $5-8 \times 10^7$ s^{-1}.[4] The density of coupling states ρ_l is estimated using the equation derived previously,[41–43]

$$\rho_l = 2cA_1/(A_2 \times k_1). \tag{2}$$

With $A_1/A_2 = 1.5$ and $k_1 = 1 \times 10^8$ s^{-1}, ρ_l is estimated to be 900 per cm^{-1}. Fast dephasing in CD_3CDO is due to greater ρ_l (about 500 per cm^{-1} for CH_3CHO) and the coupling matrix element seems not to vary for the isotopic species.

Gejo *et al.*[3] reported single exponential decays for excited acetaldehyde up to vibrational energy $E(S_1) = 2000$ cm^{-1} in S_1. The coherent width of their laser is about 100 and resolution is ~120 MHz. Given $\rho_l = 900$ per cm^{-1} at near the threshold region, within the laser bandwidth only about three eigenstates were excited. Hence, either single exponential decay or quantum-beat oscillation is expected to be observed in the fluorescence. With a multimode laser and resolution ~0.1 cm^{-1} used in this work, many more eigenstates were excited, and biexponential decay is expected because of averaging over various rates.

The fitted rate coefficient k_2 depends on the excitation energy and shows a stepwise structure similar to the appearance rate coefficients measured for both isotopic variants of acetaldehyde. This slow rate is equivalent to the rate of reversed intersystem crossing when the excitation energy is below the dissociation threshold. However, in the case of acetaldehyde, the rate of reversed intersystem crossing is slow for states with low vibrational energy in S_1, and single exponential decays are observed. When the dissociation channel opens, then k_2 is expected to reflect the dissociation rate. In the case of CH_3CHO, experimental data show that k_2 is approximately equal to the appearance rate coefficient. For CD_3CDO, k_2 starts to deviate from the coefficient for the appearance rate when excitation energy is well above the

TABLE I. Total energies E (hartree) and relative energies ΔE (cm^{-1}) with respect to ground state acetaldehyde for states S_0 and T_1 and the transition state of CH_3CHO.

	HF/6-31*		B3LYP/6-31G*		B3LYP/6-311+G*		MP2(full)/6-311+G*		G2MP2		Exptl.
	E	ΔE	E	ΔE		ΔE	E	ΔE	E	ΔE	ΔE
S_0	−152.862 626	0	−153.775 396	0	−153.821 805	0	−153.426 276	0	−153.519 463	0	0
T_1	−152.785 526	16927	−153.661 650	24973	−153.707 291	25142	−153.290 157	29885	−153.391 655	28 060	27240[a]
$TS(T_1)$	−152.737 358	27503	−153.637 857	30195	−153.686 124	29789	−153.268 128	34722	−153.378 964	30 865	31650[b]

[a]Reference 55.
[b]This work.

dissociation threshold. One possible explanation is that T_1 states are not equally coupled well to the dissociation continuum. Those states coupled to the dissociation channel are expected to have a fast decay and a fast rise in appearance of formyl radical. States not coupled well to dissociation still contribute to emission, and overall result in slower decay in curves measured for excited acetaldehyde. In CH_3CHO the density of states is smaller and coupling to the dissociation continuum is not notably different as in the case of CD_3CDO.

C. Results of *ab initio* calculations

We carried out *ab initio* calculations on energies and structures of S_0, T_1, and transition states along the path of dissociation to CH_3+HCO. Early investigation by Yadav and Goddard[9] on excited states of acetaldehyde is at the HF/3-21G level. We evaluated optimized geometries using Hartree–Fock,[46] B3LYP,[47] and MP2[48] methods with basis set 6-31G*[49] and 6-311+G*.[50] All harmonic vibrational frequencies were calculated using the analytic second derivative to confirm all stationary points. The method of intrinsic reaction coordinate (IRC)[51] was applied to determine the transition structure on the T_1 surface for the reaction $CH_3CHO \rightarrow CH_3+HCO$. All calculations were performed with the GAUSSIAN94 program.[52] Table I lists the energies calculated according to various methods. Table II presents vibrational frequencies of S_0 and T_1 states and a comparison with experimental results. Table III presents vibrational frequencies calculated for the transition state on the triplet surface. The energies of these electronic levels listed were corrected for zero-point energy and scaled according to conventional factors.[53] The calculated energies using method G2MP2[54] were scaled by 0.89. Frequencies listed were scaled by 0.989, 0.9427 for method B3LYP/6-311+G* and MP2(full)/6-311+G*, respectively.[53]

Compared with experimental data, the energies calculated using G2MP2 show the best agreement. The values using method B3LYP/6-311G* have a deviation ~8%. These two methods yield values much better than those from HF. For vibrational modes, B3LYP frequencies agree with experimental data for the S_0 state better than results from MP2(full)/6-311+G*. For the T_1 state, experimental data show that the energy difference between term values for 0^0 and 15^1 is 180 cm^{-1}, and for 0^0 and 10^1 is 400 cm^{-1},[55] ν_{15} denotes the torsional mode and ν_{10} CCO bend. Because interaction between ν_{15} and the inversion motion is strong, the measured differences among vibrational levels are scattered. In Table II these two modes correspond to ν_{15} and ν_{14}; the B3LYP frequencies are 199 and 364 cm^{-1} and MP2 frequencies are 174 and 327 cm^{-1}, respectively. For the frequency of the CCO bending mode calculated with the MP2 method, there is a large deviation from the experimental value. Over-

TABLE II. Vibrational frequencies (cm^{-1}) of T_1 and S_0 states of acetaldehyde.

	T_1				S_0		
\Method	UB3LYP/6-311+G*		UMP2(full)/6-311+G*		B3LYP/6-311+G*	MP2(full)/6-311+G*	Experimental[a]
vib.	CH_3CHO	CD_3CDO	CH_3CHO	CD_3CDO	CH_3CHO	CH_3CHO	CH_3CHO
ν_1	3092	2291	2714	1966	3104	3023	3005
ν_2	3048	2247	2679	1981	3043	2978	2967
ν_3	2957	2139	2642	1940	2992	2902	2917
ν_4	2921	2129	2599	1870	2848	2796	2822
ν_5	1488	1249	1156	1083	1793	1676	1743
ν_6	1464	1070	1284	969	1468	1420	1441
ν_7	1387	1069	1216	932	1461	1416	1420
ν_8	1252	1054	1126	925	1416	1366	1390
ν_9	1166	890	1014	809	1377	1336	1352
ν_{10}	1013	875	907	787	1124	1091	1113
ν_{11}	971	805	885	717	1122	1084	1107
ν_{12}	907	714	806	631	879	863	877
ν_{13}	618	477	568	434	769	743	763
ν_{14}	364	334	327	299	505	486	509
ν_{15}	199	150	174	131	148	134	150

[a]Reference 58.

TABLE III. Vibrational frequencies (cm^{-1}) of the transition state on the T_1 surface from *ab initio* calculations.

\Method	UB3LYP/6-311+G*		UMP2(full)/6-311+G*	
vib.	CH_3CHO	CD_3CDO	CH_3CHO	CD_3CDO
ν_1	3229	2405	2810	2092
ν_2	3221	2399	2801	2086
ν_3	3059	2169	2659	1889
ν_4	2655	1948	2273	1689
ν_5	1678	1663	1611	1574
ν_6	1417	1040	1249	914
ν_7	1407	1033	1235	905
ν_8	1058	821	981	745
ν_9	945	716	920	705
ν_{10}	773	578	758	578
ν_{11}	585	433	635	469
ν_{12}	545	394	598	437
ν_{13}	280	259	295	276
ν_{14}	118	90	151	115
ν_{15}	338 *i*	334 *i*	488 *i*	480 *i*

all, a deviation ~10% is found for B3LYP frequencies compared to those of the triplet state by comparing with these two vibrational frequencies.

Figure 13 displays the geometry of the transition state on the T_1 surface using the B3LYP method. The vectors in this figure denote displacements of individual atoms for the dissociating vibrational mode. This geometry shows an elongated C–C bond and the HCO plane is at an angle to the C–C bond. If the repulsive force originated along the C–C bond according to an impulsive model, the torque produced from dissociation would have a significant contribution to rotation of HCO along its principal rotational axis *b*; the *b* axis is in the HCO plane and approximately perpendicular to the C–O bond. These results are observed experimentally in that fragment HCO has rotation preferentially excited along the *b* axis.[8]

D. RRKM fits to dissociation of acetaldehyde

Moore and co-workers[19,20] and Ionov *et al.*[21] observed vibrational frequencies pertaining to transition states along the dissociation path of triplet ketene and NO_2, respectively. Evidence for quantization of the transition state for isomerization of *cis*- and *trans*-1,2,5,7,-octatetraene was reported.[23] All these results show that vibrational modes orthogonal to the reaction coordinate remain relatively quantized in the transition state. These vibrational levels are still well defined at the saddle point on the dissociating surfaces. In the case of acetaldehyde for which absorption to the S_1 state is still discrete, no peak in both PHOFEX and fluorescence excitation spectra was found to correspond to steps in the plots of appearance rate versus excitation energy for both isotopic species. Hence we tentatively assign these features in the plots to vibrational levels of the transition state.

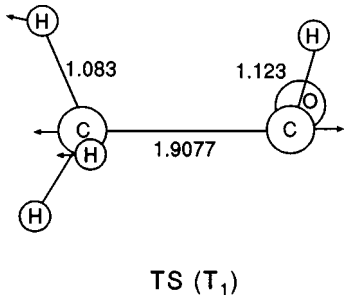

FIG. 13. *Ab initio* geometry of the transition state on the T_1 surface of CH_3CHO calculated with the B3LYP method.

We use the transition state version of RRKM theory defined by

$$k(E)=\frac{P(E-E_{\text{threshold}})}{h\rho(E)}, \tag{3}$$

in which $P(E)$ is the transmission probability for each quantized reaction threshold on the transition state. The transmission probability using an inverted parabola and an Eckart barrier gives about the same results in fitting the experimental data. Here, we assume that the rotation quantum numbers are conserved through the dissociation. ρ is calculated with the Whitten–Rabinovitch equation.[22] As dissociation occurs along the triplet surface, we used the calculated vibrational frequencies of the T_1 state listed in Table II to estimate the density of dissociating states. We assume $\rho(E)=f\times\rho_{\text{W-R},T_1}(E)$ to enable varying parameter f to fit the experimental curves. The fits to experimental curves are shown in Fig. 8. Near the top of the barrier, $\rho_{\text{W-R},T_1}(E)$ is 430 and 150 per cm^{-1} with B3LYP frequencies for CD_3CDO and CH_3CHO, respectively and 1040 and 270 per cm^{-1} with MP2 frequencies. The vibrational frequencies for the transition states listed in Table III were used in the calculations. The best RRKM fit of f value is ~7 for CD_3CDO and ~8 for CH_3CHO when B3LYP frequencies are used. The methyl torsional mode is considered to be almost a rotational motion; then the calculated ρ becomes increased and a small f value is expected. Including anharmonicity, the f value can be further decreased. Compared to the value $\rho_l=900$ per cm^{-1} estimated from the biexponential decay, deviation of the calculated $\rho_{\text{W-R},T_1}$ value is about 100% using the vibrational frequencies with method B3LYP and about 10% with MP2. Near the dissociation threshold, ρ_l estimated from the dephasing rate is smaller than the value obtained from RRKM fits.

An imaginary frequency $\sim 60i$ cm^{-1} much smaller than the calculated value is found to produce the best fit to the data for both isotopic variants of acetaldehyde. Similar results were reported for triplet ketene. An explanation is that the shape near the saddle point is rather anharmonic and using one frequency to describe the shape of the potential is inadequate. From fitting spacings in experimental curves, the vibrational frequencies are $\nu_{14}=(73\pm10)$ cm^{-1} and $\nu_{13}=(200\pm10)$ cm^{-1} for CD_3CDO and $\nu_{14}=(80\pm10)$ cm^{-1} for CH_3CHO. They are assigned as the torsional mode of methyl ν_{14} and C–C–O bend ν_{13}, respectively. These values are much smaller than *ab initio* values using methods B3LYP and MP2 (full) but near the scaled values for CH_3CHO, $\nu_{14}=87$ and $\nu_{13}=249$ cm^{-1} calculated by Yadav and Goddard.[9] The values calculated with density functional theory tend to deviate from experimental data especially for

excited states. Hence, for a transition state, deviations are expected. However, values obtained with method MP2 have greater deviations than those with B3LYP.

These results indicate that vibrational modes in acetaldehyde seem not to promote dissociation significantly because the dissociation rate increases monotonically with excitation energy except for these stepwise structures. Selecting a different part of a vibronic band can excite various rotational states in S_1 of acetaldehyde. In Fig. 10 the ratio A_1/A_2 shows a minimum at wavelengths 315.3, 314.25, and 313.4 nm. These positions correspond to peaks of vibronic bands in the PHOFEX spectrum. Transitions to rotational states with small rotational quantum number J are near the peak position given the perpendicular band type typically observed for the S_1-S_0 transition of acetaldehyde. Hence, small A_1/A_2 value around the peak region indicates that states with small J states tend to interact with a fewer number of the triplet states than the states with large J. Similarly, Gejo *et al.*[3] observed that interaction of S_1 and T_1 states depends on rotational quantum number J. Overall, because of the low temperature applicable to a molecular jet, only states with small J are populated. Hence, from experimental data the variation of the rate of appearance from states with various J is small such that a stepwise structure due to the vibrational level in the transition state can be observed.

From RRKM fits, the top of the dissociation barrier is determined to be $E_{th}=31\ 650\ \mathrm{cm}^{-1}$ (316.00 nm) and 31 840 cm^{-1} (314.10 nm) for CH_3CHO and CD_3CDO, respectively. A lower threshold is found for CH_3CHO than for the deuterated species because of disparate zero-point energies. HCO was observed with photolysis wavelengths greater than the dissociation threshold because relatively warm jets were used in this work. Dissociation occurring from the S_0 surface is reported for formaldehyde.[56,57] However, the rate of dissociation from this surface in acetaldehyde is expected to be slow because the density of S_0 states is large, $\sim 10^8$. Hence, according to experimental results the triplet channel becomes a dominant pathway for formation of the radical products soon after the energy reaches the threshold. Kono *et al.*[7] determined the appearance threshold of HCO to 320.5 nm. Ohta *et al.*[40] reported the threshold to be 317.3 for CH_3CHO and 316.0 nm for CD_3CDO. Gejo *et al.*[3] estimated the threshold of CH_3CHO to be ~314.8 nm using quantum-beat data. The determined threshold varies with the experimental conditions. Contribution from hot bands can lower the dissociation threshold. Our method using the RRKM fit should be more accurate.

V. CONCLUSIONS

Although both PHOFEX and excitation spectra show partially resolved rotational structures they do not correspond to the sharp increases in the plot of appearance rate versus excitation energy. The threshold of dissociation for formation of radical fragments is determined accurately using the RRKM model by fitting sharp increases of the rate of appearance of formyl radicals to a vibrational level of the transition state on the triplet surface. Vibrational spacings in the transition state are obtained by measuring either the decay of the excited state correlated to dissociation or the rate of appearance of fragments even if the process of absorption is discrete. Limited by the temporal resolution of our laser, a few vibrational levels in transition state near the top of dissociation barrier were observed. A picosecond laser system is expected to resolve further vibrational frequencies via measuring the decay rate of highly vibrational states of S_1. Deuterated acetaldehyde has a dephasing rate greater than that of CH_3CHO due to greater density of coupling states. The coupling matrix element between S_1 and T_1 in the energy region of interest varies insignificantly with isotopic species.

From comparison of measured vibrational levels in transition states with calculated values, the geometry of the transition state given by calculation in this work is too tight. Further investigation of state-resolved dynamics can elucidate problems such as conservation of rotational quantum number K and specificity of vibrational mode to dissociation. The spectroscopy of acetaldehyde at energies near the dissociation limit is important in relation to investigation of the effect of various vibrational modes and rotational states in promoting dissociation.

ACKNOWLEDGMENT

We thank the National Science Council of the Republic of China (Contract No. NSC 87-2113-M-007-34) for support.

[1] D. A. Hansen and E. K. C. Lee, J. Chem. Phys. **63**, 3272 (1975).
[2] M. Noble and E. K. C. Lee, J. Chem. Phys. **80**, 134 (1984).
[3] T. Gejo, H. Bitto, and J. R. Huber, Chem. Phys. Lett. **261**, 443 (1996).
[4] S.-H. Lee and I-C. Chen, Chem. Phys. **220**, 175 (1997).
[5] T. Kono, M. Takayanagi, T. Nishiya, and I. Hanazaki, Chem. Phys. Lett. **201**, 166 (1993).
[6] T. Kono, M. Takayanagi, and I. Hanazaki, J. Phys. Chem. **97**, 12,793 (1993).
[7] A. C. Terentis, M. Stone, and S. H. Kable, J. Phys. Chem. **98**, 10,802 (1994).
[8] S.-H. Lee and I-C. Chen, J. Chem. Phys. **105**, 4597 (1996).
[9] J. S. Yadav and J. D. Goddard, J. Chem. Phys. **84**, 2682 (1986).
[10] A. Horowitz, C. J. Kershner, and J. G. Calvert, J. Phys. Chem. **86**, 3094 (1982).
[11] A. Horowitz and J. G. Calvert, J. Phys. Chem. **86**, 3105 (1982).
[12] S. Speiser, W. F. Pfeiffer, and G. H. Atkinson, Chem. Phys. Lett. **93**, 480 (1982).
[13] A. K. Sappey and D. R. Crosley, J. Chem. Phys. **93**, 7601 (1990).
[14] T. A. Cool and X.-M. Song, J. Chem. Phys. **96**, 8675 (1992).
[15] J. D. Tobiason, J. R. Dunlop, and E. A. Rohlfing, J. Chem. Phys. **103**, 1448 (1995).
[16] G. W. Adamson, X. Zhao, and R. W. Field, J. Mol. Spectrosc. **160**, 11 (1993).
[17] S.-H. Lee and I-C. Chen, J. Chem. Phys. **103**, 104 (1995).
[18] S.-H. Lee and I.-C. Chen, J. Chem. Phys. **105**, 2583 (1996).
[19] E. R. Lovejoy, S. K. Kim, and C. B. Moore, Science **256**, 1541 (1992).
[20] S. K. Kim, E. R. Lovejoy, and C. B. Moore, J. Chem. Phys. **102**, 3202 (1995).
[21] S. I. Ionov, G. A. Brucker, C. Jaques, Y. Chen, and C. Wittig, J. Chem. Phys. **99**, 3420 (1993).
[22] P. J. Robinson and K. A. Holbrook, *Unimolecular Reactions* (Wiley, New York, 1971).
[23] Y. S. Choi, T.-S. Kim, H. Petek, K. Yoshihara, and R. L. Christensen, J. Chem. Phys. **100**, 9269 (1994).
[24] P. G. Wenthold, D. A. Hrovat, W. T. Borden, and W. C. Lineberger, Science **272**, 1456 (1996).
[25] A. H. Zewail, Science **242**, 1646 (1988).
[26] J. C. Polanyi and A. H. Zewail, Acc. Chem. Res. **28**, 119 (1995).
[27] E. S. Medvedev and D. W. Pratt, J. Chem. Phys. **105**, 3366 (1996).
[28] M. Noble, E. C. Apel, and E. K. C. Lee, J. Chem. Phys. **78**, 2219 (1983).

[29] M. Noble and E. K. C. Lee, J. Chem. Phys. **81**, 1632 (1984).
[30] M. Baba, I. Hanazaki, and U. Nagashima, J. Chem. Phys. **82**, 3938 (1985).
[31] R. A. Weersink, D. T. Cramb, S. C. Wallace, and R. D. Gordon, J. Chem. Phys. **102**, 623 (1995).
[32] J. M. Price, J. A. Mack, G. v. Helden, X. Yang, and A. M. Wodtke, J. Phys. Chem. **98**, 1791 (1994).
[33] H. Liu, E. C. Lim, R. H. Judge, and D. C. Moule, J. Chem. Phys. **102**, 4315 (1995).
[34] H. Liu, E. C. Lim, C. Muñoz-Caro, A. Niño, R. H. Judge, and D. C. Moule, J. Mol. Spectrosc. **175**, 172 (1996).
[35] S.-H. Jen, T.-J. Hsu, and I-C. Chen, Chem. Phys. **231**, 131 (1998).
[36] S.-H. Lee and I-C. Chen, *Proceeding of the SPIE Conference on Laser Techniques for State Selected and State-to-State Chemistry III*, San Diego, 1995, edited by J. W. Hepburn (SPIE, Bellingham, WA, 1995).
[37] N. Ohta and H. Baba, J. Phys. Chem. **90**, 2654 (1986).
[38] C. Stöck, X. Li, H.-M. Keller, R. Schinke, and F. Temps, J. Chem. Phys. **106**, 5333 (1997).
[39] M. Noble and E. K. C. Lee, J. Chem. Phys. **80**, 134 (1984).
[40] N. Ohta, T. Koguchi, T. Takemura, and I. Suzuka, Chem. Phys. Lett. **191**, 232 (1992).
[41] R. v. d. Werf, D. Zevenhuijzen, and J. Kommandeur, Chem. Phys. Lett. **27**, 325 (1974).
[42] R. v. d. Werf and J. Kommandeur, Chem. Phys. **16**, 125 (1976).
[43] R. v. d. Werf and J. Kommandeur, Chem. Phys. **16**, 151 (1976).
[44] A. Frad, F. Lahmani, A. Tramer, and C. Tric, J. Chem. Phys. **60**, 4419 (1974).
[45] F. Lahmani, A. Tramer, and C. Tric, J. Chem. Phys. **60**, 4431 (1974).
[46] H. B. Schlegel, J. Comput. Chem. **3**, 214 (1982); C. C. J. Roothan, Rev. Mod. Phys. **23**, 69 (1951).
[47] A. D. Becke, J. Chem. Phys. **98**, 5648 (1993).
[48] M. J. Frisch, M. Head-Gordon, and J. A. Pople, Chem. Phys. Lett. **166**, 275 (1990); **166**, 281 (1990); J. A. Pople, R. Krishnan, H. B. Schlegel, and J. S. Binkley, Int. J. Quantum Chem., Symp. **13**, 325 (1979); N. C. Handy and H. F. Schaefer III, J. Chem. Phys. **81**, 5031 (1984).
[49] R. Ditchfield, W. J. Hehre, and J. A. Pople, J. Chem. Phys. **54**, 724 (1971).
[50] A. D. McLean and G. S. Chandler, J. Chem. Phys. **72**, 5639 (1980); R. Krishnan, J. S. Binkley, R. Seeger, and J. A. Pople, *ibid.* **72**, 650 (1980); K. Raghayachariand and G. W. Trucks, *ibid.* **91**, 1062 (1989); T. Clark, J. Chandrasekhar, G. W. Spitznagel, and P. v. R. Schleyer, J. Comput. Chem. **4**, 294 (1983).
[51] C. Gonzalez and H. B. Schlegel, J. Chem. Phys. **90**, 2154 (1989); J. Phys. Chem. **94**, 5523 (1990).
[52] M. J. Frisch, G. W. Trucks, H. B. Schlegel, P. M. W. Gill, B. C. Johnson, M. A. Robb, J. R. Cheeseman, T. A. Keith, G. A. Petersson, J. A. Montgomery, K. Raghavachari, M. A. Al-Laham, V. G. Zakrzewski, J. V. Ortiz, J. B. Foresman, C. Y. Peng, P. Y. Ayala, M. W. Wong, J. L. Andres, E. S. Replogle, R. Gomperts, R. L. Martin, D. J. Fox, J. S. Binkley, D. J. Defrees, J. Baker, J. P. Stewart, M. Head-Gordon, C. Gonzalez, and J. A. John, Gaussian, Inc., Pittsburgh, PA, 1995.
[53] L. A. Curtiss, K. Raghavacharari, and J. A. Pople, J. Chem. Phys. **98**, 1293 (1993).
[54] J. B. Foresman and A. Frisch, *Exploring Chemistry with Electronic Structure Methods*, 2nd ed. (Gaussian, Pittsburgh, PA 1996).
[55] H. Liu, E. C. Lim, C. Muñoz-Caro, A. Niño, R. H. Judge, and D. C. Moule, J. Chem. Phys. **105**, 2547 (1996).
[56] M.-C. Chuang, M. F. Foltz, and C. B. Moore, J. Chem. Phys. **87**, 3855 (1987).
[57] A. C. Terentis, S. E. Waugh, G. F. Metha, and S. H. Kable, J. Chem. Phys. **108**, 3187 (1998).
[58] T. Shimanouchi, *Tables of Molecular Vibrational Frequencies*, Publication NSRDS, Natl. Stand. Rep. Data Serv., Natl. Bur. Stand. Circ. No. 39 (U.S. GPO, Washington, D.C., 1972).